Technical Report
RAL-TR-2000-013

Calibration of the Electron Volt Spectrometer, a Deep Inelastic Neutron Scattering Spectrometer at the ISIS Pulsed Neutron Spallation Source

A L Fielding and J Mayers

April 2000

COUNCIL FOR THE CENTRAL LABORATORY OF THE RESEARCH COUNCILS

The Central Laboratory of the Research Councils
Library and Information Services
Rutherford Appleton Laboratory
Chilton
Didcot
Oxfordshire
OX11 0QX
Tel: 01235 445384 Fax: 01235 446403
E-mail library@rl.ac.uk

ISSN 1358-6254

Calibration of the electron Volt spectrometer, a deep inelastic neutron scattering spectrometer at the ISIS pulsed neutron spallation source

A.L. Fielding[$]

Department of Physics, University of Liverpool, Oxford street, Liverpool L69 7ZE, UK.

J. Mayers

Rutherford Appleton Laboratory, Chilton, Didcot, Oxon, OX11 0QX, UK.

[$]Address for correspondence*: ISIS Facility, Rutherford Appleton Laboratory, Chilton, Didcot, Oxon, OX11 0QX, UK.*

Abstract

The electron Volt spectrometer (eVS) is an inverse geometry filter difference spectrometer that has been optimised to measure the single atom properties of condensed matter systems using a technique known as neutron Compton scattering (NCS) or deep inelastic neutron scattering (DINS). The spectrometer utilises the high flux of epithermal neutrons that are produced by the ISIS neutron spallation source enabling the direct measurement of atomic momentum distributions and ground state kinetic energies. In this paper the procedure that is used to calibrate the spectrometer is described . This includes details of the method used to determine detector positions and neutron flight path lengths as well as the determination of the instrument resolution. Examples of measurements on 3 different samples are shown, ZrH_2, ^4He and Sn which show the self-consistency of the calibration procedure.

1. Introduction

The electron Volt spectrometer (eVS) is an inelastic neutron scattering instrument at the ISIS pulsed neutron spallation source that has been optimised to measure the single particle properties of condensed matter systems. The eVS allows the direct measurement of the atomic momentum distribution, n(p) and single particle mean kinetic energies. The technique is unique in this respect having been used successfully to obtain values of the mean atomic kinetic energies in solid and liquid helium [1,2], other noble gases in solid and liquid phases [3], hydrogen bonds [4], metals [5], liquid and solid hydrogen [6], glasses [7], graphite [8], molecular solids [9] and metal hydrides [10].

Hohenberg and Platzmann [11] first suggested measuring atomic momentum distributions in condensed matter by high energy neutron scattering; they were motivated by the possibility of measuring the Bose condensate in superfluid liquid Helium-4. The technique, known as neutron Compton scattering (NCS) or deep inelastic neutron scattering (DINS) relies on the impulse approximation (IA) being valid. The IA states that if the energy, ω and momentum transfer, q are sufficiently large then the scattering can be considered to occur from a single nucleus with kinetic energy and momentum being conserved. The formal statement of the IA for a system containing only particles of mass M can be written

$$S_M(\boldsymbol{q},\omega) = \int n(\boldsymbol{p})\delta\left(\omega - \frac{(\boldsymbol{p}+\boldsymbol{q})^2}{2M} + \frac{p^2}{2M}\right)d\boldsymbol{p} \qquad [1]$$

where $n(\boldsymbol{p})d\boldsymbol{p}$ is the probability that an atom has momentum in the volume element $d\boldsymbol{p}$ centred at $\boldsymbol{p}$. The terms in the parentheses represent the conservation of kinetic energy. Therefore, in the IA the measured quantity $S(\boldsymbol{q},\omega)$, the incoherent dynamic scattering function can be directly related to the atomic momentum distribution.

In this regime of scattering the momentum and energy transfer can be considered to be coupled by *y*-scaling [12]; *y* is the component of atomic momentum $\boldsymbol{p}$, along the direction of $\boldsymbol{q}$ and M is the mass of the target atom.

$$y = \mathbf{p}.\hat{\mathbf{q}} = \frac{M}{q}\left(\omega - \frac{q^2}{2M}\right) \qquad [2]$$

Measurement of a large number of scattering events yields the longitudinal neutron Compton profile, J(*y*) which can be considered as a one dimensional projection of the atomic momentum distribution n($\boldsymbol{p}$) along the direction of $\boldsymbol{q}$ and is the probability that an atom has a component of momentum between *y* and dy. It follows from equations 1 and 2 that

$$S_M(\boldsymbol{q},\omega) = \frac{M}{q}J(y) \qquad [3]$$

The mean single atom kinetic energy can also be derived directly from the second moment of J(*y*).

The measured count rate in a time channel of width Δt centred at time-of-flight t is [13],

$$C(t)\Delta t = \left(I(E_0)\frac{dE_0}{dt}\Delta t\right)\left[\eta(E_1)\Delta\Omega\Delta E_1\right]\sum_M N_M \frac{d^2\sigma_M}{d\Omega dE_1} \qquad [4]$$

The first term in parentheses is the intensity of incident neutrons with times of flight between t and t+Δt. The second factor is the product of the detector efficiency η at energy E_1, the detector solid angle $\Delta\Omega$ and the energy resolution ΔE_1 and is a constant determined by the instrument geometry and the type of detector. The third factor is the product of N_M, the number of atoms of mass M in the sample and the double differential scattering cross-section for mass M, summed over all atomic masses present in the sample. The double differential scattering cross-section for scattering from mass M is [14]

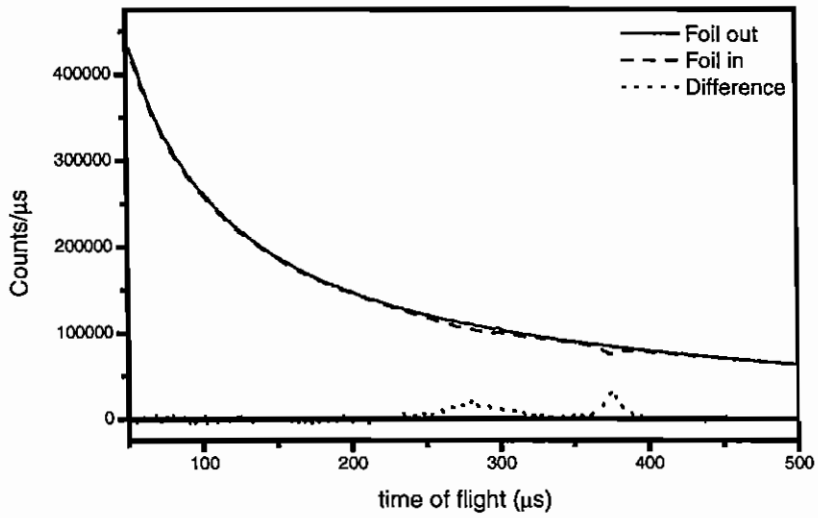

Figure 1 *Plot of the foil in and foil out scattering data measured from a* ZrH_2 *sample. Also plotted is the foil out – foil in difference spectra showing the well separated peaks due to the scattering from the Zr and H atoms in the sample.*

$$\frac{d^2\sigma_M}{d\Omega dE_1} = b_M^2 \frac{v_1}{v_0} S_M(q,\omega) = b_M^2 \frac{v_1}{v_0}\frac{M}{q} J_M(y_M) \qquad [5]$$

where b_M is the scattering length of atoms of mass M and equation 3 has been used. Taking into account the finite instrument resolution function an expression for the measured count rate can be obtained

$$C(t) = \frac{v_1 \eta(E_1)\Delta\Omega\Delta E_1 I(E_0) dE_0/dt}{v_0} \sum_M N_M b_M^2 M J_M(y_M) \otimes R_M(y_M) \qquad [6]$$

where $\otimes$ denotes a convolution and $R_M(y_M)$ is the (mass dependent) instrument resolution function in momentum space. The term before the summation is entirely sample independent and is determined purely by the instrument geometry and measured t. The measured count rate can therefore be related directly to neutron Compton profile, J(y).

The eVS is an inverse geometry time-of-flight spectrometer that uses a filter difference technique to define the final neutron energy. The incident neutron beam is a white beam from the ambient temperature water moderator at the ISIS source. The final neutron energy, E_1, is defined using thin foils that have strong neutron absorption resonance's in the eV energy range. On eVS gold or uranium-238 foils are used. The analyser foils are cycled in and out of the scattered neutron beam at five minute intervals. The foil in and foil out data are stored in separate areas of the computers memory and a difference taken. The difference signal represents the spectrum of neutrons scattered with a final energy equal to the absorption resonance energy of the analyser foils. Figure 1 shows an example of foil in and foil out data measured from a zirconium hydride sample. The two peaks correspond to the recoil scattering from the light hydrogen nuclei (centred at ~280 μs) and the heavier zirconium nuclei (centred at ~375 μs), the centre of the peak corresponds to the mass dependent recoil energy of the nuclei ,ω_R.

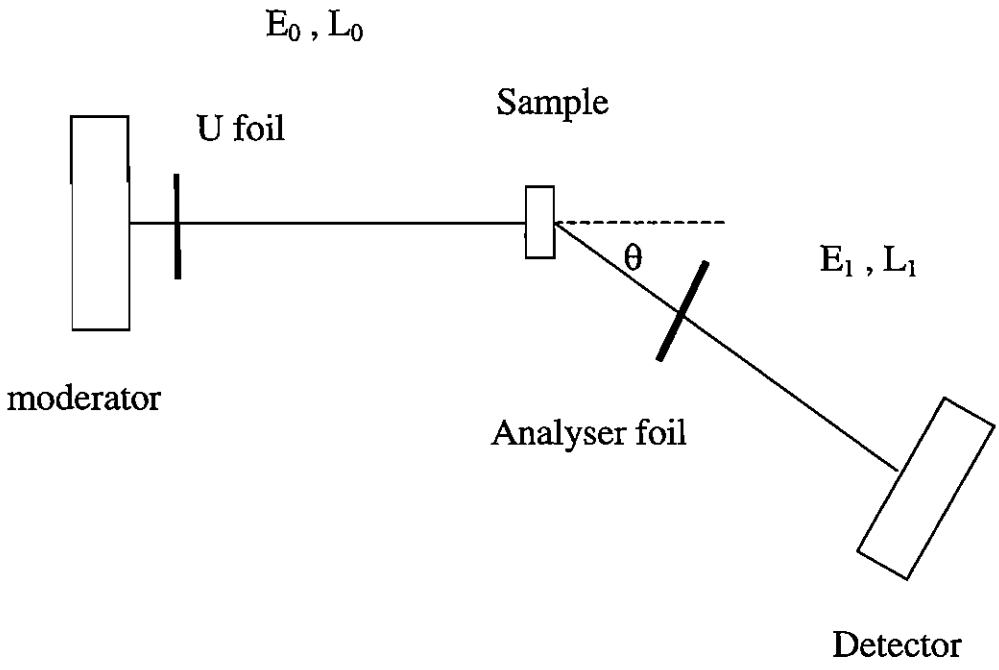

Figure 2 *Schematic diagram of the eVS spectrometer.*

The peaks shown in the difference spectrum of figure 1 have two contributions to their width. The first is a Doppler broadening effect due to the atomic vibration which is physically of interest as in the IA it can be directly related to the atomic momentum distribution. The second contribution to the width is the broadening due to the instrument resolution. Calibration of the eVS can be split into two parts. Firstly, the detector positions need to be known accurately if the measured time-of-flight is to be related to the energy and momentum transfers. Secondly, it is important that the instrument resolution is known accurately if accurate physical information is to be derived from the measured time-of-flight signal. In this paper the calibration method used to derive the instrument parameters defining the detector positions and instrument resolution is described.

2. Principal of the calibration procedure of the eVS

The neutron time-of-flight is defined as the time taken, starting from the instant the neutron leaves the moderator, for the neutron to travel along the incident beam tube, scatter from the sample and then travel to the detector. Figure 2 shows a schematic diagram of the instrument indicating the five physical parameters that define the neutron time-of-flight. They are the initial and final neutron flight paths, L_o and L_1, the scattering angle θ, the initial and final neutron energies E_o and E_1. The neutron time-of-flight can thus be written

$$t - t_o = \frac{L_o}{v_o} + \frac{L_1}{v_1} \qquad [7]$$

where t_o is a timing constant that determines which channel in the time-of-flight spectrum corresponds to (infinitely fast) neutrons with zero time-of-flight. This is determined by electronic delay times in the detector-discriminator-Electronics-computer chain. These five instrument parameters are required for the calculation of the momentum transfer q and energy transfer ω of a neutron with time-of-flight t to the target atoms in the sample. A lead sample is chosen for calibration measurements for a number of reasons,

(1) It has a narrow intrinsic width due to the atomic momentum distribution such that the measured signal will be dominated by the instrument resolution.
(2) The large mass of the Pb atoms means that there is very little recoil so that the scattering is almost elastic.
(3) The low Debye temperature of Pb (T_D = 88 K) means that at room temperature the system can be considered to be classical (to within 0.1 %) and hence the kinetic energy is simply given by $3/2k_BT$.

To calibrate the eVS spectrometer, two measurements with a Pb sample are required;

U foil calibration: A measurement is performed on the Pb sample with a thin U foil in the incident neutron beam. The analyser foils remain out of the scattered beam for this run. This run is used to determine the detector positions, defined by a scattering angle, θ and final neutron flight path length, L_1. The eVS at present has thirty two lithium doped glass scintillator detectors arranged in four banks of eight.

Pb calibration: A measurement is performed on the Pb sample with the U foil out of the incident neutron beam. The U or Au analyser foils are cycled in and out of the scattered beam during this measurement. This measurement is used to calibrate the final neutron energy E_1 and energy resolution σ_{E1} defined by the neutron absorption resonance(s) of the analyser foils.

The initial flight path L_o is known from physical measurements (L_o = 11.055 m) but could in fact be found from the shift in the neutron Compton profile of ^{4}He from y = 0. The total flight path ($L_o + L_1$) for each detector can be determined by measuring the positions of resonance absorption lines in the time-of-flight spectrum for scattering from a thin lead sample. A thin uranium foil is placed in the incident beam, close to the moderator. Uranium has four strong well defined neutron absorption resonance's at 6671, 20872, 36680 and 66020 meV that have been studied extensively and are know to a very good accuracy (1 % level) [15]. For elastic scattering the time-of-flight is given by equation 7 with $\nu_1 = \nu_0$ but for recoil scattering a correction needs to be made, since $\nu_1 < \nu_0$. For recoil scattering from lead at neutron energies greater than 5eV the impulse approximation is valid and the change in neutron velocity is

determined only by the conservation of kinetic energy and momentum. Hence, the ratio of the final neutron velocity to the initial neutron velocity is a function of the scattering angle θ and atomic mass M and can be written

$$\frac{v_1}{v_0} = \mathrm{R}(\theta) = \frac{\cos\theta + \sqrt{(\mathrm{M}/\mathrm{m})^2 - \sin^2\theta}}{(\mathrm{M}/\mathrm{m}) + 1} \qquad [8]$$

Thus, from equations 7 and 8

$$\mathrm{t} = \mathrm{t}_o + [\mathrm{L}_o + \mathrm{L}_1 / \mathrm{R}(\theta)] / v_o \qquad [9]$$

By plotting the times of flight of the absorption lines for the uranium resonance's against $1/v_0$ and performing a least squares fit, the gradient obtained is $L_0 + L_1 / R(\theta)$ and the y-intercept will give the time delay constant t_0.

The eVS spectrometer also simultaneously functions as a time-of-flight diffractometer with a continuous spectrum of initial wavelengths. The wavelength λ of a neutron is related to its velocity v through the de Broglie relation

$$\lambda = \hbar / \mathrm{m}v \qquad [10]$$

Bragg peaks will be present in a spectra from a detector at a given angle θ when Bragg's law is satisfied

$$2d \sin(\theta/2) = n\lambda \qquad [11]$$

Bragg scattering is elastic so that $v_0 = v_1 = v$ and from equation 7

$$v = (L_0 + L_1)/(t - t_0) \qquad [12]$$

Using equations 10 and 12 a relationship between the measured time-of-flight at which Bragg peaks from a lead calibration sample with known d-spacing occur and the scattering angle can be obtained

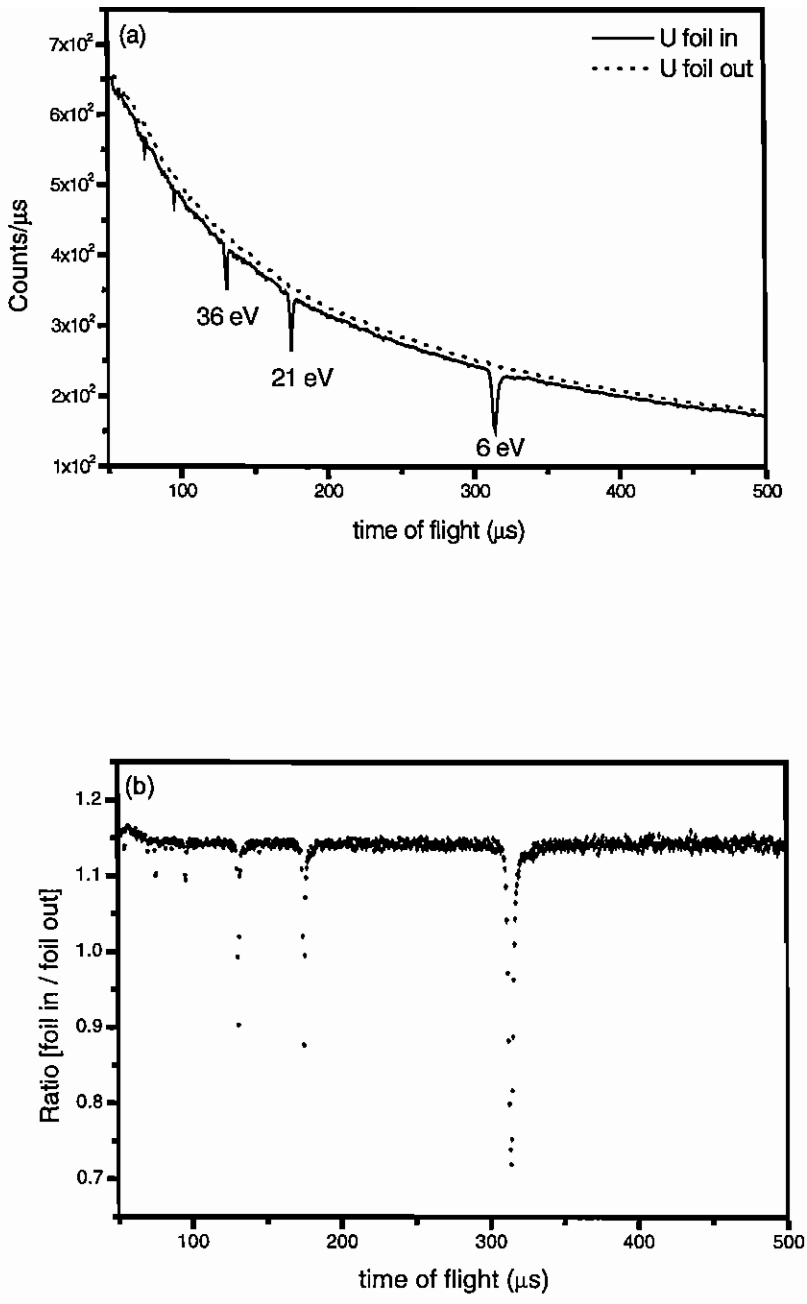

Figure 3 *(a) The scattering from a Pb sample with (solid line) and without (dashed line) a thin uranium foil in the incident beam. The analyser foils were out of the scattered beam for this measurement.*

(b) The ratio of the U foil in and U foil out data.

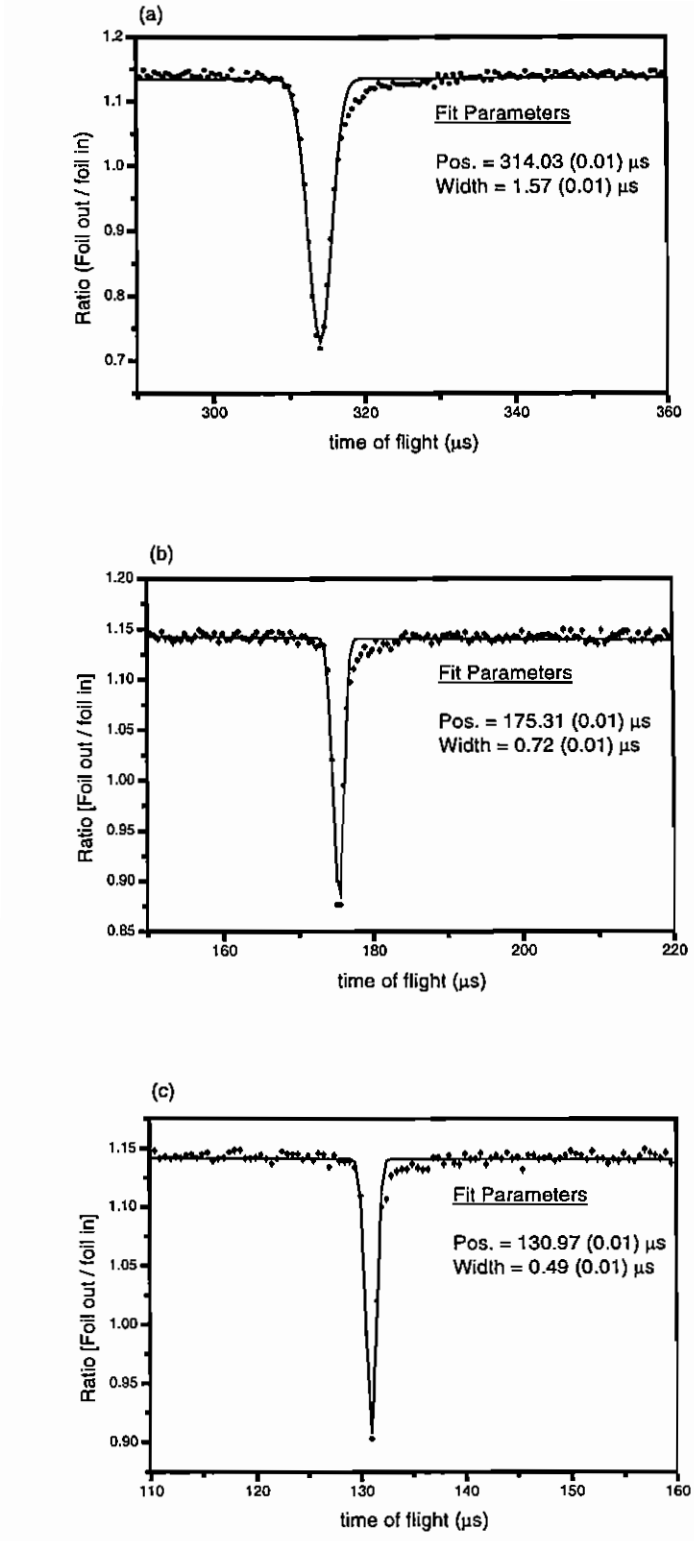

Figure 4 *The Gaussian fits to the U foil data shown in figure 3. Shown are the fits to the (a) 6 eV, (b) 21 eV and (c) 36 eV resonance's .*

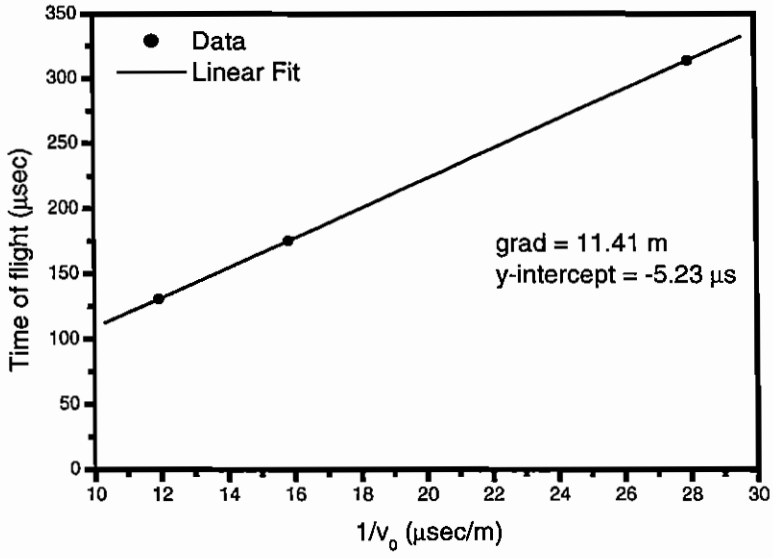

Figure 5 *The fitted positions in time-of-flight plotted as a function of $1/v_0$ where v_0 is the incident neutron velocity corresponding to the three resonance's. The straight line is a least squares fit to these points from which the neutron flight path ($L_0 + L_1$) and the t_0 term can be derived.*

$$2d\sin\left(\frac{\theta}{2}\right) = \frac{n\hbar(t - t_0)}{m(L_0 + L_1)} \qquad [13]$$

Since the scattering angle θ must be known for an accurate measurement of L_1 , but L_1 must be also known for an accurate calibration of θ it is necessary to use an iterative procedure. For scattering from lead (M= 207.19 amu), R(θ) varies between 1 for θ = 0° and ≈ 0.99 for θ = 180°. Hence, θ can be given an arbitrary value to derive L_1 and t_0 from equation 9. Using these values of L_1 and t_0 and equation 13 a more accurate value for θ may be determined, the values of L_1 and t_0 can be then be re-calculated. This procedure converges rapidly such that these three steps are sufficient for an accurate calibration of the instrument flight paths and scattering angles.

3. Example of the calibration procedure

3.1. Flight path and t_0 calibration

Figure 3(a) shows the data from a single detector for the two Pb sample calibration runs described in the previous section. The solid line shows data from the U foil calibration run and is the signal measured with the U foil in the incident beam. The dashed line shows the signal with the U foil removed. The dips in the spectrum are due to the neutron absorption resonance's of the uranium foil, the 3 lowest energy resonance's are labelled and these are used in the calibration procedure. A ratio of the foil in and foil out signals is then taken and this is shown in figure 3(b). The three lowest energy resonance's are then fitted with Gaussian functions to obtain the position in time-of flight and also the width. The fits and derived parameters are shown in figure 4. The asymmetry in the low intensity tails of the resonance is possibly due to neutron multiple scattering effects in the detector scintillator glass. This contribution has been found to be small enough (less than 1 % level) to be neglected. This procedure provides the positions in time of flight of the 3 neutron absorption resonance's which are then plotted as time-of-flight against $1/v_0$ where v_0 is the initial neutron velocity. A least squares linear fit of equation 9 is performed to the time of flight against $1/v_0$ and is shown in figure 5. An arbitrary choice of scattering angle θ can be made since R(θ), in equation 9, varies between 0.99 and 1,

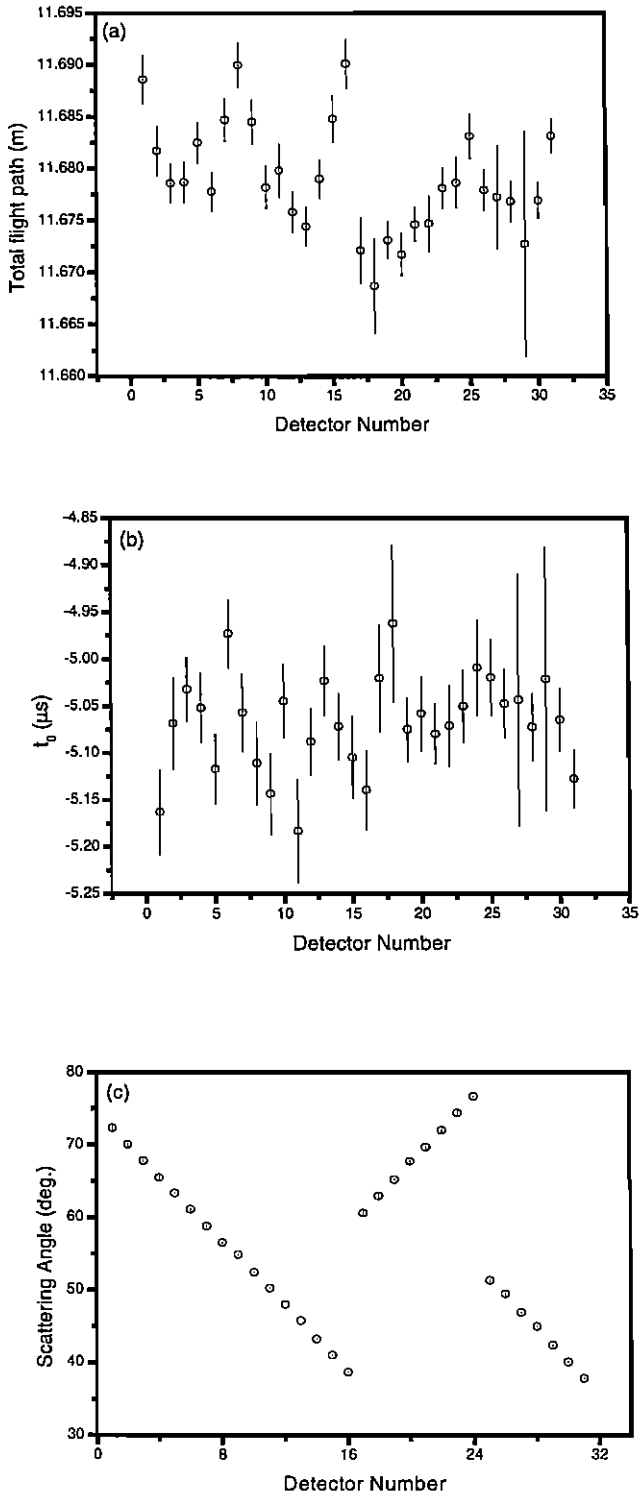

Figure 6 (a) *The calibrated flight paths plotted as a function of the detector number. (b) the calibrated t_0 values plotted as a function of detector number. (c) The calibrated detector angles plotted as a function of detector number.*

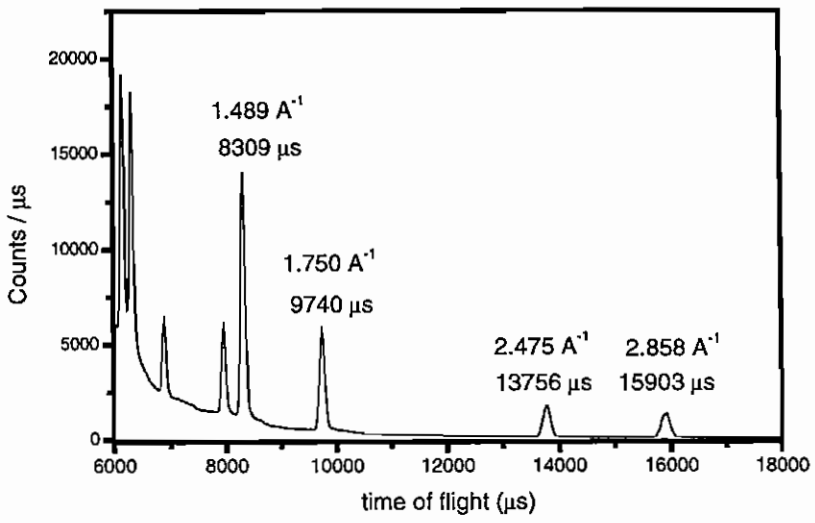

Figure 7 *The diffraction spectra measured on eVS from the Pb calibration sample. The detector scattering angles are derived from the positions of the diffraction peaks in the time-of-flight spectra.*

allowing the final neutron flight path to be derived from the gradient and the t_0 time-of-flight correction from the y-intercept. From the fitted gradient (equal to 11.41) one can infer that the final flight path from the sample to the detector is equal to 0.355 m (the initial flight path is well known from previous measurements). Each detector is calibrated independently using this procedure. Figure 6 shows the calibrated (a) total flight path L and (b) t_0 value for each detector. The error bars on the points show that flight paths can be calibrated to an accuarcy of a few millimetres.

3.2 Angle calibration

Once values for L_1 and t_0 have been obtained then one can use these values in equation 13 to derive a more accurate value for the scattering angle θ. Figure 7 shows the Bragg scattering peaks from the Pb calibration sample. The *d*-spacing of these 4 Bragg peaks for the highest angle detector are shown in table 1 along with the measured time-of-flight of the peaks. The recorded time-of-flight values for the 4 lowest order Bragg peaks (longest time-of-flight) measured in each detector are then used (in equation 13) to calculate the mean scattering angle for each detector. Figure 6 (c) shows the calibrated angle for each detector.

***D* –spacing (Å)**	**Time-of-flight (μs)**
1.489	8309
1.750	9740
2.475	13756
2.858	15903

Table 1 *The d-spacing and measured time-of-flight for the 4 longest d-spaced Bragg peaks for the Pb calibration sample.*

This completes the calibration of the detector positions so that an instrument parameter (IP) file can be produced containing the detector number, scattering angle θ, t_0 correction, initial neutron flight path L_0 and the final neutron flight path L_1.

4. E_1 Calibration and the Resolution function

4.1 The eVS resolution function

The instrument parameters discussed in the previous section are average values, and hence for each parameter there is a distribution of values. For example, the initial flight path L_o of the neutron is uncertain because of the finite depth of the moderator. Also, the parameters L_1 and θ will have a distribution of possible values due to the finite detector and sample size, E_1 will have a range of possible values due to the width of the absorption resonance peak of the analyser foil and t_o will have a range of possible values due to inaccuracies in the measurement of the time-of-flight. A probability distribution exists for each parameter and the shape of these distributions determines the shape of the instrument resolution function [16].

To a good approximation all the parameter probability distributions except for the energy resolution component (for Au analyser foils) can to a good approximation be considered Gaussian, *i.e.* for parameter x (L_o, L_1, θ or t_o) the probability distribution is given by

$$P(x) = \frac{1}{\sqrt{2\pi\Delta x^2}} \exp\left(\frac{-(x - \langle x \rangle)^2}{2\Delta x^2}\right) \qquad [14]$$

where $\langle x \rangle$ is the mean value of the parameter and Δx is the standard deviation of the distribution. The energy distribution $P(E_1)$ is assumed to be Gaussian for uranium analyser foils and Lorentzian for gold analyser foils. For the latter case

$$P(E_1) = \frac{\Delta E_1}{\pi} \frac{1}{(E_1 - \langle E_1 \rangle)^2 + \Delta E_1^2} \qquad [15]$$

where ΔE_1 is the half-width-at-half-maximum.

The effect of these distributions is to broaden the measured response in time-of-flight. Since the time-of-flight spectrum can be directly related to the atomic momentum distribution through y-scaling, shown in equations 2 - 6, then the y-transformed

neutron Compton profile, $J(y)$, will also be resolution broadened. The measured response in y-space is in fact a convolution of the intrinsic neutron Compton profile $J(y)$ and the resolution function $R(y)$. It is thus necessary to know the resolution function to a high degree of accuracy if meaningful information is to be extracted from the Compton profile. The resolution function $R(y)$ is made up of contributions from the five instrument parameters described previously that can be related by

$$R(y) = R_\theta(y) * R_{L0}(y) * R_{L1}(y) * R_t(y) * R_E(y) \qquad [16]$$

where $R_\theta(y)$ is the angular, $R_{L0}(y)$ is the L_0, $R_{L1}(y)$ is the L_1, $R_t(y)$ is the time, $R_E(y)$ is the energy component of the resolution in y-space and $*$ indicates a convolution. As already described, the distributions for the angular, initial and final flight paths and time components of the resolution are represented by Gaussians and hence characterised by their standard deviations σ_θ, σ_{L0}, σ_{L1} and σ_t respectively. The four standard deviations can be added in quadrature to give the total Gaussian contribution σ_G to the width of the resolution function

$$\sigma_G^2 = \sigma_\theta^2 + \sigma_{L0}^2 + \sigma_{L1}^2 + \sigma_t^2 \qquad [17]$$

The energy contribution in y-space to the resolution is dependent on the type of analyser foil used. Gold foils give a Lorentzian distribution that will be characterised by the half-width-at-half-maximum of the distribution while uranium analyser foils have a Gaussian distribution of energies that are characterised by the standard deviation. The overall resolution function is defined by a Voigt function *i.e.* a convolution of a Gaussian with a Lorentzian, if gold analyser foils are used, or for uranium analyser foils a Gaussian with a standard deviation given by

$$\sigma_{total}^2 = \sigma_G^2 + \sigma_E^2 \qquad [18]$$

The following sections show how the σ values are derived from measurements or calculation.

4.1. Flight path and time resolution

The value of ΔL_0 is determined by measuring the transmission of a thin uranium foil in the incident beam using the two monitor counters which are situated at 8.6 m, the incident beam monitor and 13.44 m, the downstream monitor, from the moderator. Gaussian fits are made to the dips in the transmitted spectrum and these yield a position and a width σ (standard deviation) for each resonance energy. It is assumed that the measured width is made up of three Gaussian components,

(1) The intrinsic energy width of the U-foil absorption ΔE. In time-of-flight this corresponds to $\sigma_{tE} = (L/v)(\Delta E/2E)$ where $v = \sqrt{2m_n E}$ is the neutron velocity corresponding to energy E. The energies and the intrinsic widths of the absorption peaks can be calculated from the foil thickness and tabulated nuclear resonance parameters [17] and are listed for the five lowest energy absorption resonance's in table 2.

(2) The uncertainty in the measured time-of-flight, Δt_0. This is due to a combination of jitter in the electronics and the time bin width (usually 0.25 μs).

(3) The uncertainty in the flight path ΔL. For the monitor detectors, which are very thin, the uncertainty is entirely due to the finite moderator depth and so is equal to the uncertainty in the initial flight path, ΔL_0. This has a width in time-of-flight given by $\sigma_{tL} = \Delta L/v$.

E_1	ΔE_1
6677 meV	53.0 meV
20878 meV	95.0 meV
36688 meV	142.0 meV
66034 meV	145.0 meV
102558 meV	198.4 meV

Table 2 *E_1 is the energy and ΔE_1 the fitted Gaussian standard deviation of the resonance absorption peak in a uranium foil with 1.456×10^{20} atoms/cm^2*

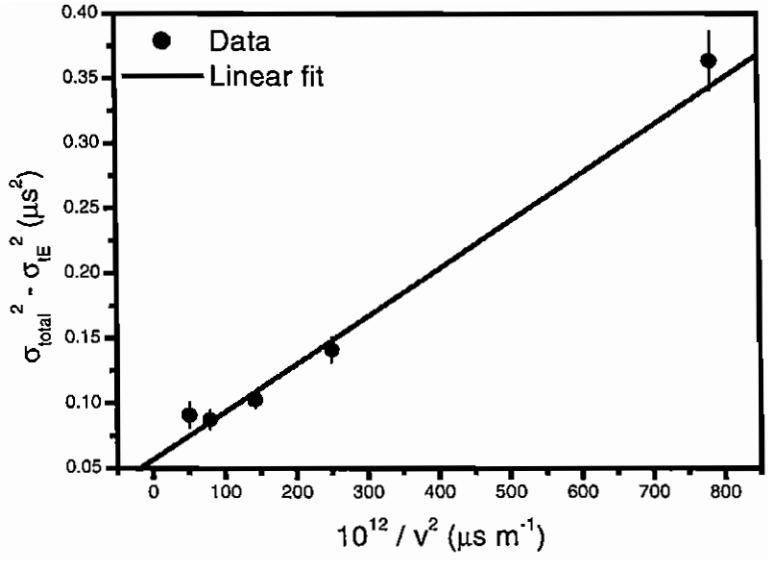

Figure 8 *The fitted widths of the U foil resonance's as a function of $1/v^2$ where v is equal to $\sqrt{2mE_R}$ and E_R is the resonance energy. The linear least squares fit is also plotted.*

With the assumption of a Gaussian peak shape, these widths add in quadrature, so that the measured width is

$$\sigma^2_{\text{total}} = \frac{\Delta L^2}{v_1^2} + \frac{L^2}{v_1^2}\frac{\Delta E_1^2}{4E_1^2} + \Delta t_0^2 \qquad [19]$$

Thus, a least squares fit of $\sigma_{\text{total}}{}^2$ against $1/v_1{}^2$, the value of $\Delta L = \Delta L_0$ can be determined from the gradient and Δt_0 from the intercept. A plot of $\sigma_{tL0}{}^2$ against $1/v^2$ is shown in figure 8 along with the least squares linear fit. This was performed for both monitor detectors and the derived ΔL_0 and Δt_0 values are listed in table 3. The values of ΔL_0 and Δt_0 derived independently from the two monitors agree within error, indicating that the calibration procedure works well.

	ΔL_0 (cm)	Δt_0 (μs)
Monitor 1	1.75 ± 0.21	0.30 ± 0.03
Monitor 2	2.16 ± 0.20	0.26 ± 0.03

Table 3 *The initial flight path uncertainty, ΔL_o and time uncertainty Δt_o for both the monitor detectors.*

To determine ΔL_1 and Δt_0 an analogous procedure is followed. A uranium foil is inserted in the incident beam and Gaussian fits are made to the widths and positions of the resonance peaks after scattering from a lead sample into each of the detectors. In this case the value of ΔL derived from a least squares fit of equation 19 is the uncertainty in the total flight path.

$$\Delta L^2 = \Delta L_0{}^2 + \Delta L_1{}^2 \qquad [20]$$

The mean values of the total flight path uncertainty and time uncertainty for each bank of detectors derived using this procedure are shown in table 4. Since ΔL_0 has already been found from the fits to the monitor spectra, ΔL_1 is equal to $\sqrt{(2.91^2 - 2.1^2)}$ = 2.0 cm .

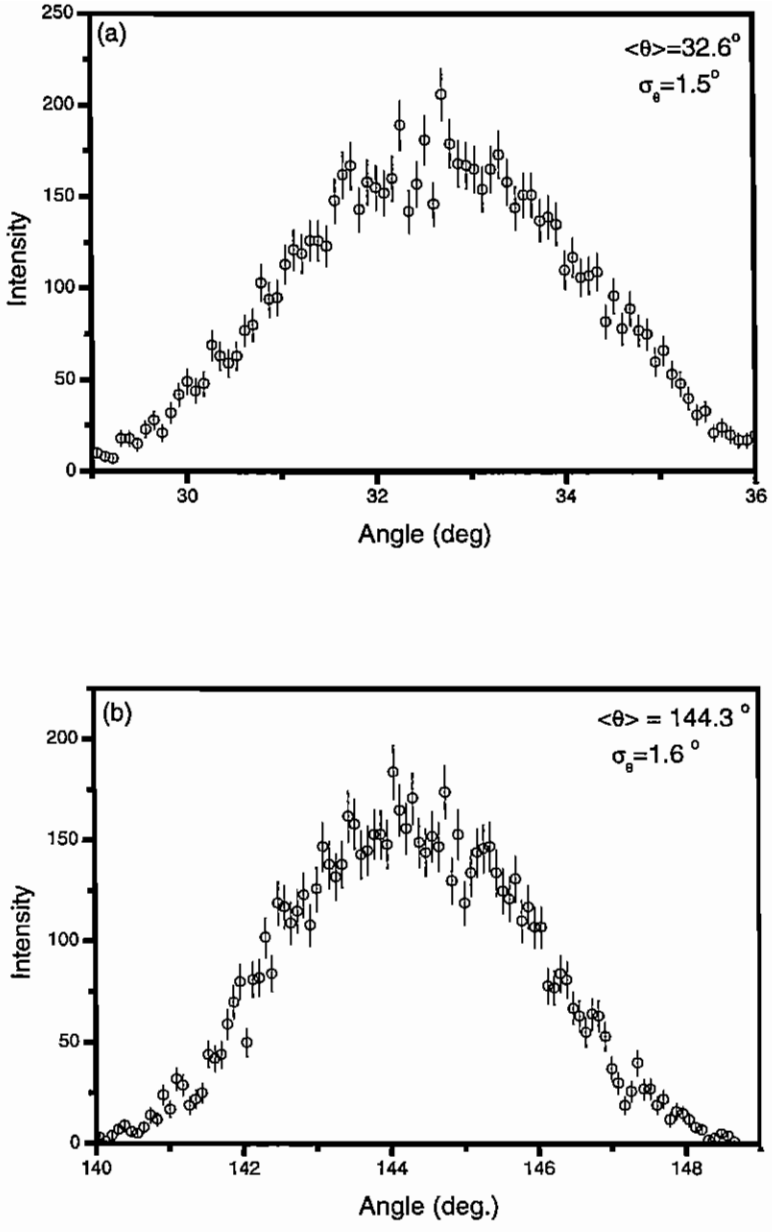

Figure 9 *The calculated distribution of scattering angles for (a) a low angle detector and (b) a high angle detector.*

Detectors	ΔL (cm)	Δt_0 (μs)
1-8	3.02 (0.07)	0.28 (0.02)
9-16	2.89 (0.09)	0.26 (0.01)
17-24	2.93 (0.11)	0.27 (0.03)
25-32	2.71 (0.11)	0.33 (0.04)
1-32	2.90 (0.05)	0.28 (0.01

Table 4 *The mean total flight path uncertainty ΔL and time uncertainty Δt_o for each bank of detectors.*

4.2 Angular resolution

The range of scattering angles subtended by a particular detector is determined by the detector, sample and source sizes. $\Delta\theta$ is calculated using a Monte-Carlo program which takes into account the finite moderator, detector and sample sizes. The angular resolution is expressed in terms of the effective detector width w which is equal to $2L_1\Delta\theta$. The effective detector width varies slightly with scattering angle and L_1, mainly due to the effects of the detector height and has its minimum value for $\theta = 90°$. Figure 9 shows the calculated angular distributions of scattered neutrons for low and high scattering angle detectors.

4.3 Energy calibration and resolution

Once the parameters L_o, L_1, θ and t_o are known along with their associated probability distributions the energy E_1 can be determined from the scattering from a Pb calibration sample. The time-of-flight spectra are converted to momentum space by assuming the final neutron energy E_1 to be equal to the values determined accurately from neutron cross-section measurements.

The momentum distribution of Pb at room temperature is well described by a Debye model (since the Debye temperature of Pb is 88 K, the kinetic energy of Pb atoms at

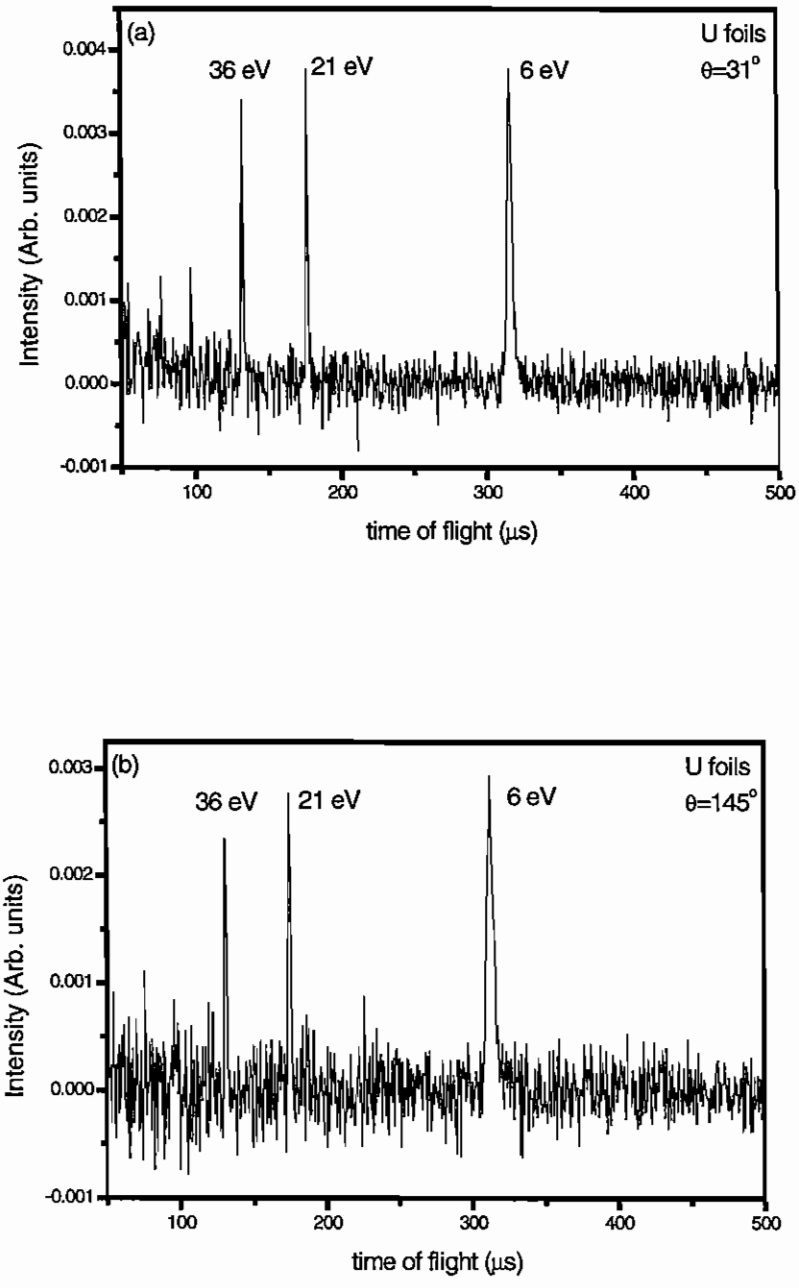

Figure 10 *Time of flight spectra measured for a Pb calibration sample with U foils at (a) low and (b) high angle.*

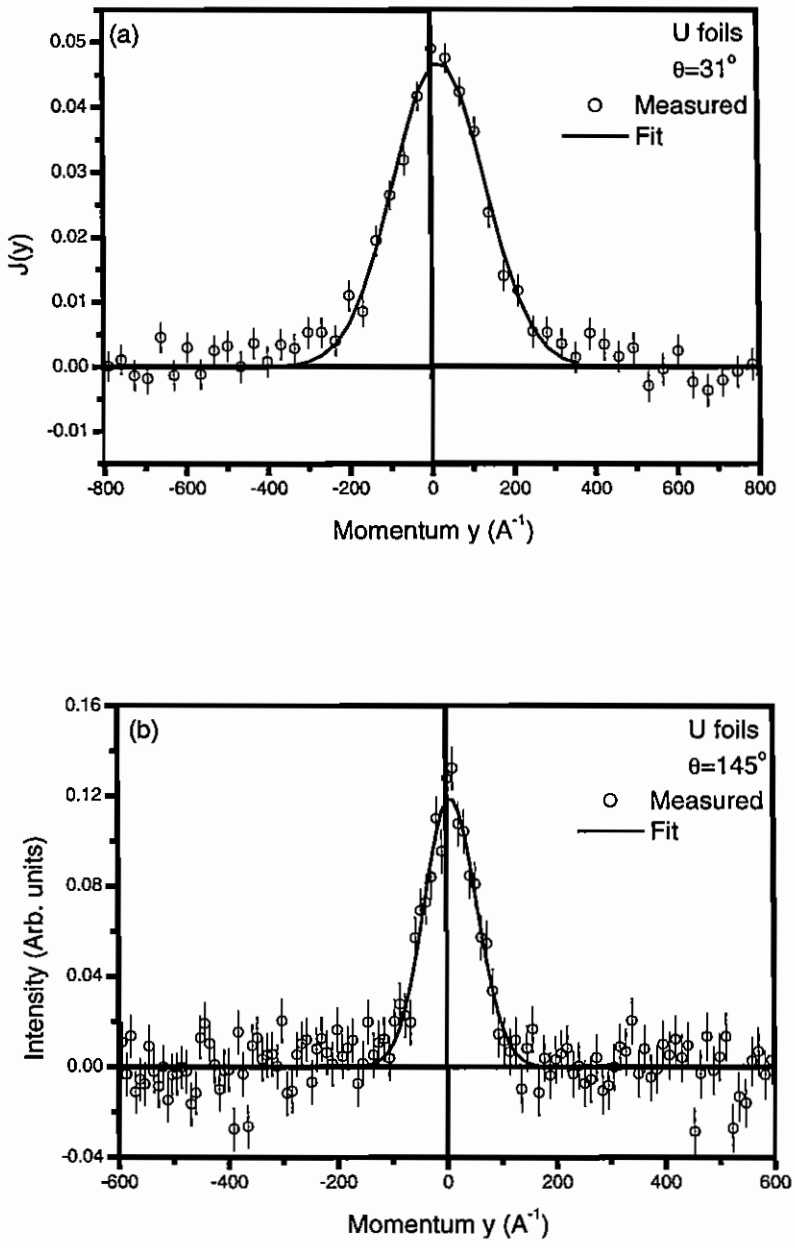

Figure 11 *The lowest energy resonance (6.6 eV) recoil peak transformed to y-space and measured at (a) low and (b) high scattering angle. The fitted Gaussian is also shown. The shift in the peak position from y=0 is used to derive a calibrated E_1 value and the fitted width σ_{E1} is used to define the energy resolution. A similar procedure is used to calibrate the two higher energy resonance peaks.*

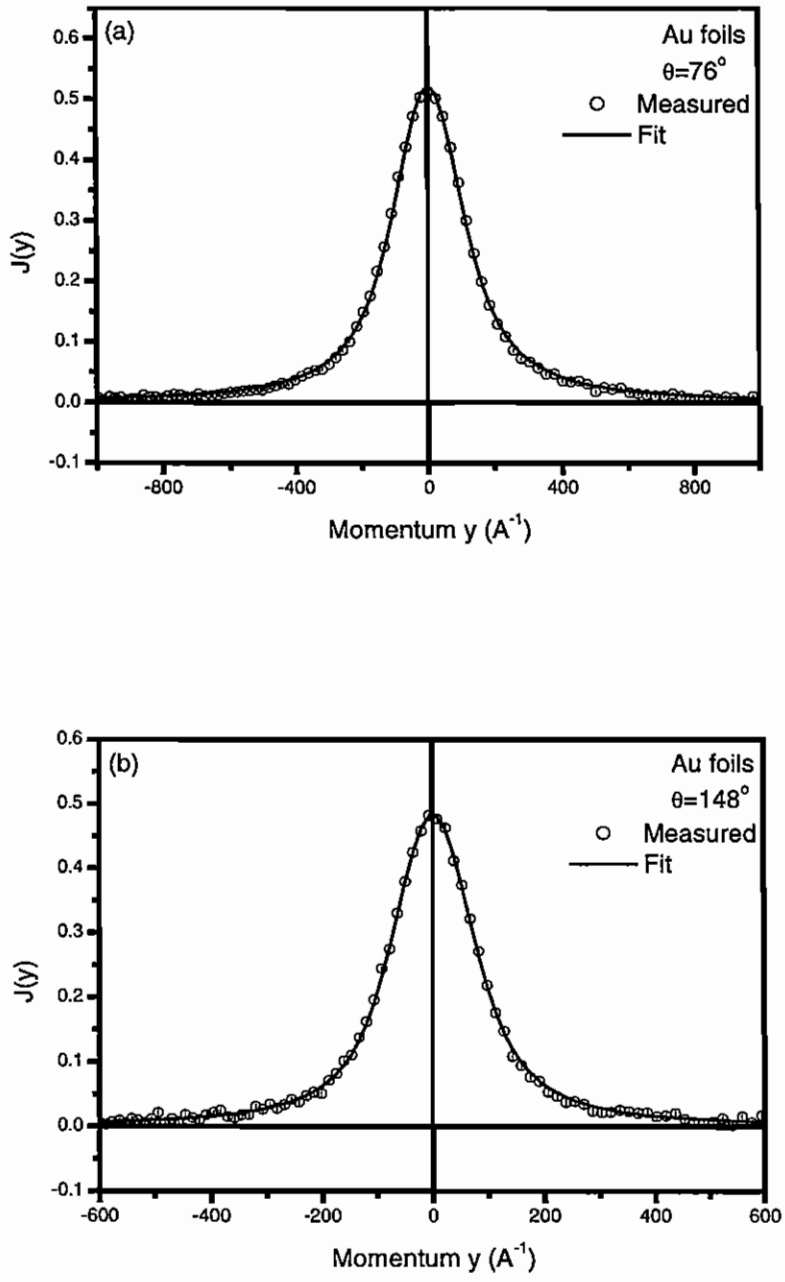

Figure 12 *The measured neutron Compton profiles for the Pb calibration sample using Au foils at (a) low and (b) high scattering angle.*

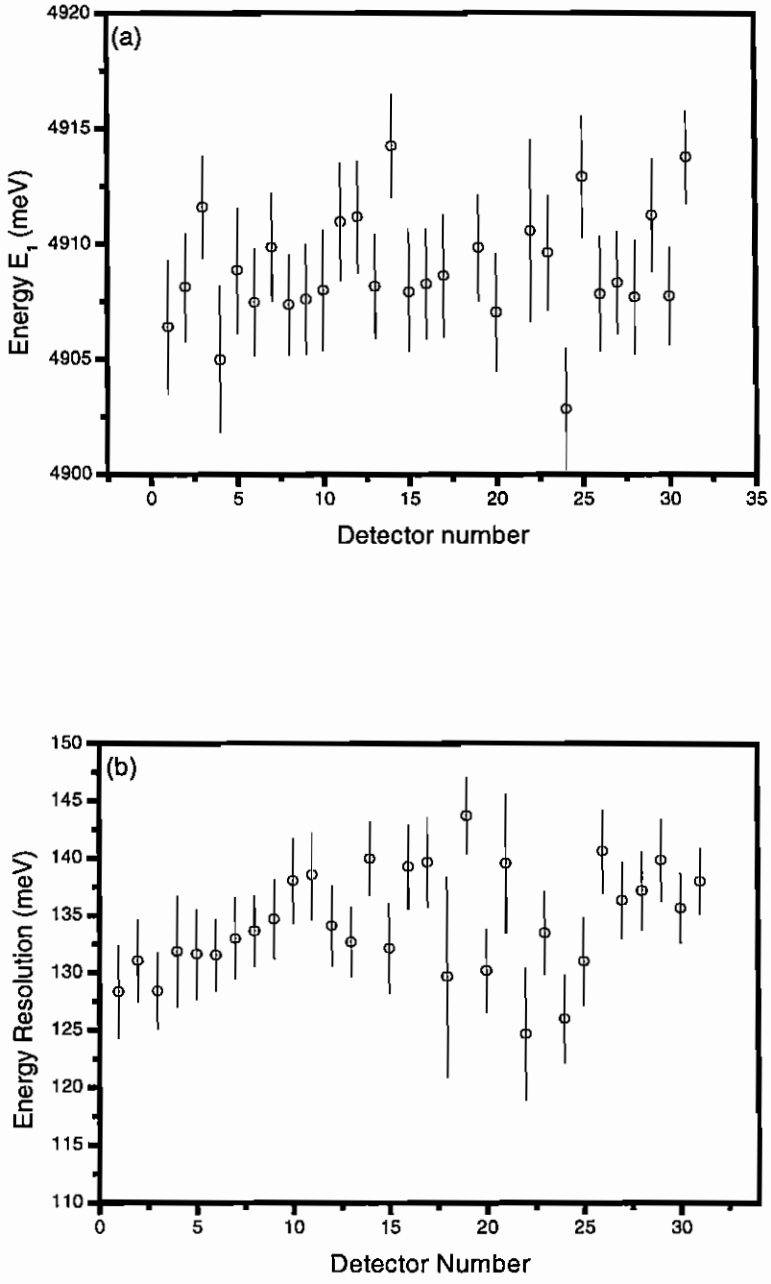

Figure 13 *The calibrated (a) energy resonance values and (b) resonance widths (half-width-at-half maximum) for the Au analyser foils for each of the 32 scintillator detectors.*

room temperature differs by only 0.1 % from the classical value of 3/2 kT and even if the density of states is not Debye-like the assumed momentum distribution should still be highly accurate). The second moment of the neutron Compton profile, σ, assuming a Debye density of states is calculated to be 35.5 Å^{-1}. As already discussed, all resolution components, other than that due to the absorption resonance line shape for Au (assumed to be Lorentzian), are assumed to have a Gaussian line shape. To determine a mean value and width for the U foil energy resonance the Pb data is fitted in y-space with a Gaussian, with all other Gaussian contributions (including the Pb sample dependent Doppler broadening) fixed. Figure 10 shows the measured time of flight difference spectra for a Pb calibration dataset using Uranium analyser foils. The data is then transformed to y-space for each of the 3 energy resonance's. The measured Compton profile using the 6.6 eV resonance is shown in figure 11 along with the fitted Gaussian. This is done for each of the resonance's. The shift in the fitted position of the peak from y = 0 is used to calculate the calibrated E_1 value of the resonance and the width gives the Gaussian σ_{E1} of the resonance. A similar procedure is carried out if gold analyser foils are used except the resonance energy width is defined by a Lorentzian half-width-at-half-maximum. Figure 12 shows plots of the measured Compton profiles for a Pb calibration run using gold analyser foils along with the fitted Voigt functions. Typical calibrated energy values for the uranium foils are E_1 = 6676 meV with σ_{E1} = 62 meV and for gold foils E_1 = 4907 meV with a hwhm = 127 meV. Each detector is energy calibrated independently in this way, the fitted E_1 and width values are shown as a function of detector in figure 13 for the gold foils. This procedure is able to calibrate the energy resonance to an accuracy of a few meV and has been proved over many years to be extremely reproducible.

5. Examples of eVS measurements

The results of a series of measurements on 3 different condensed matter systems are now briefly described. The aim of this section is to illustrate how the calibration procedure described in this paper can be used to reliably and consistently calibrate the electron Volt spectrometer to a level of accuracy that allows the measurement of atomic momentum distributions and mean single atom kinetic energies. In this section

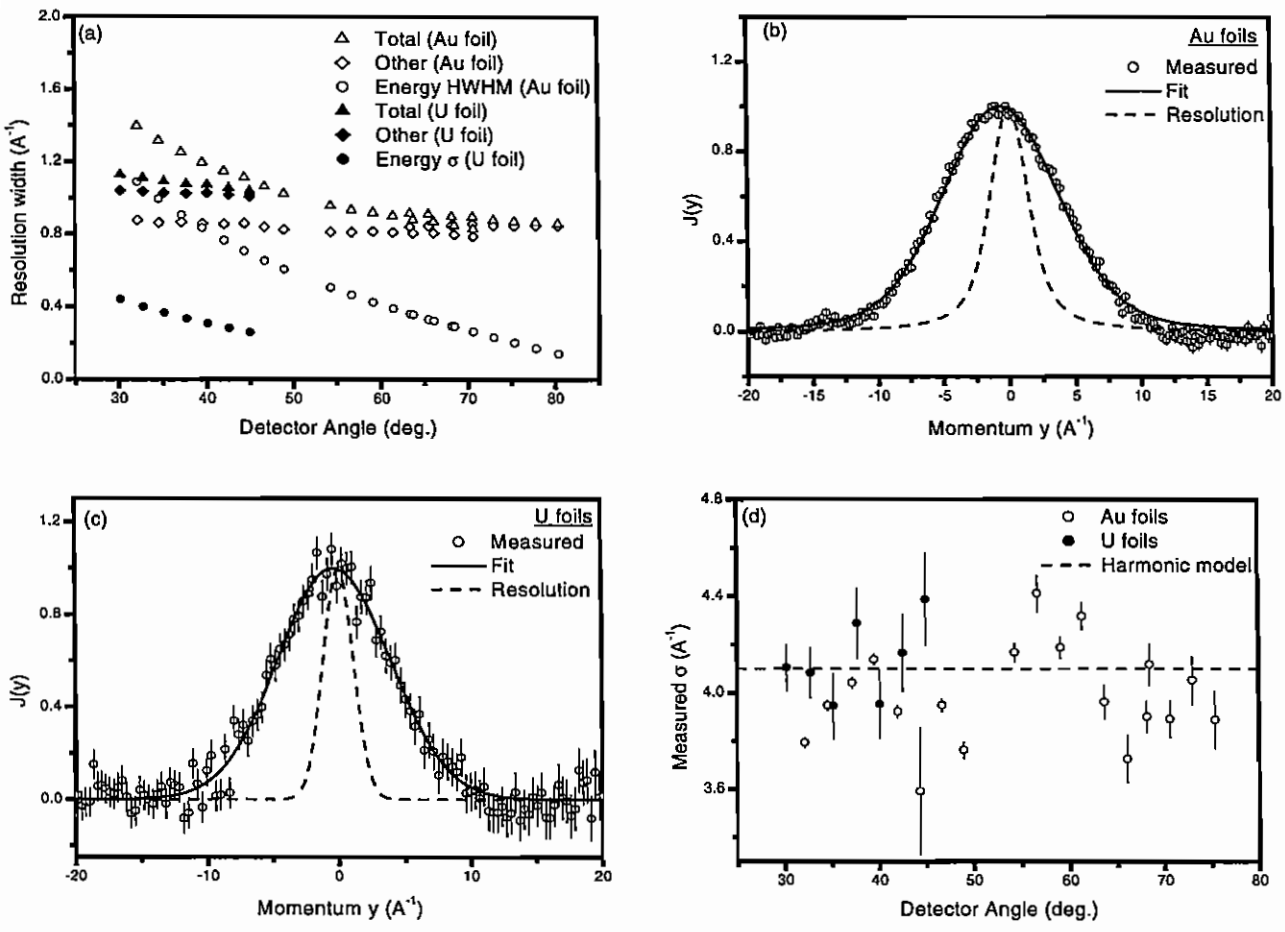

Figure 14 *(a) Resolution widths in momentum space for measurements on hydrogen in ZrH_2 as a function of scattering angle. One of the low angle banks of detectors used U analyser foils, the other three used Au analyser foils. The "other" contributions to the resolution include the uncertainties in the flight paths, L_0 and L_1, the time resolution and angular resolution. These are all assumed to be Gaussian and hence defined using a Gaussian standard deviation. (b) Neutron Compton profile for hydrogen in ZrH_2 measured with Au analyser foils at a scattering angle of 32°. The dashed line is the Voigt resolution function and the solid line is the fit to the data. (c) Neutron Compton profile for hydrogen in ZrH_2 measured with U analyser foils at a scattering angle of 30 °. The dashed line is the Gaussian resolution function and the solid line is the fit to the data. (d) The fit derived second moments of the neutron Compton profiles, J(y), plotted as a function of detector angle. The dashed line represents the value calculated in the harmonic approximation using the measured density of states.*

the emphasis is on the derived kinetic energies, more details of the data analysis and experimental method can be found in the references [10,18]

5.1 Zirconium Hydride

Measurements were made on a powder sample of zirconium hydride (ZrH_2) at room temperature using the eVS. The interest in this type of measurement is the kinetic energy of the proton in the zirconium lattice. The proton vibrations are known, to a good approximation, to be harmonic making the system ideal for testing the calibration procedures. The four banks of detectors were set-up to cover scattering angles in the range 30 – 80°. Table 5 lists the scattering angles covered by each of the banks of detectors.

Detectors	**Detector Angles**	**Analyser Foil**	**Mean σ ($Å^{-1}$)**
1 - 8	80 - 60 °	Au	3.93 (0.04)
9 - 16	44 – 30 °	U	4.13 (0.06)
17 - 24	48 – 32 °	Au	3.90 (0.06)
25 - 32	54 – 70 °	Au	4.12 (0.07)
1 - 32	32 – 80 °	Au + U	4.03 (0.04)

Table 5 *The mean second moments of the measured Compton profiles of hydrogen in ZrH_2 for each bank of detectors.*

One of the detector banks covering low scattering angles use uranium analyser foils, the other three banks use gold analyser foils. The resolution widths in momentum space are plotted as a function of scattering angle in figure 14(a). For hydrogen measurements the resolution is dominated by the angular resolution contribution. The energy resolution becomes increasingly more significant at low scattering angles for the detectors using the Au analyser foil. Figure 14 (b) and (c) show measured neutron Compton profiles at the lowest scattering angles for the Au and U analyser foils respectively. The resolution in y-space is also plotted to give a measure of how the resolution compares with the measured intrinsic Compton profile, J(y). The measured Compton profile data for each detector was fitted with a Gaussian J(y) convoluted

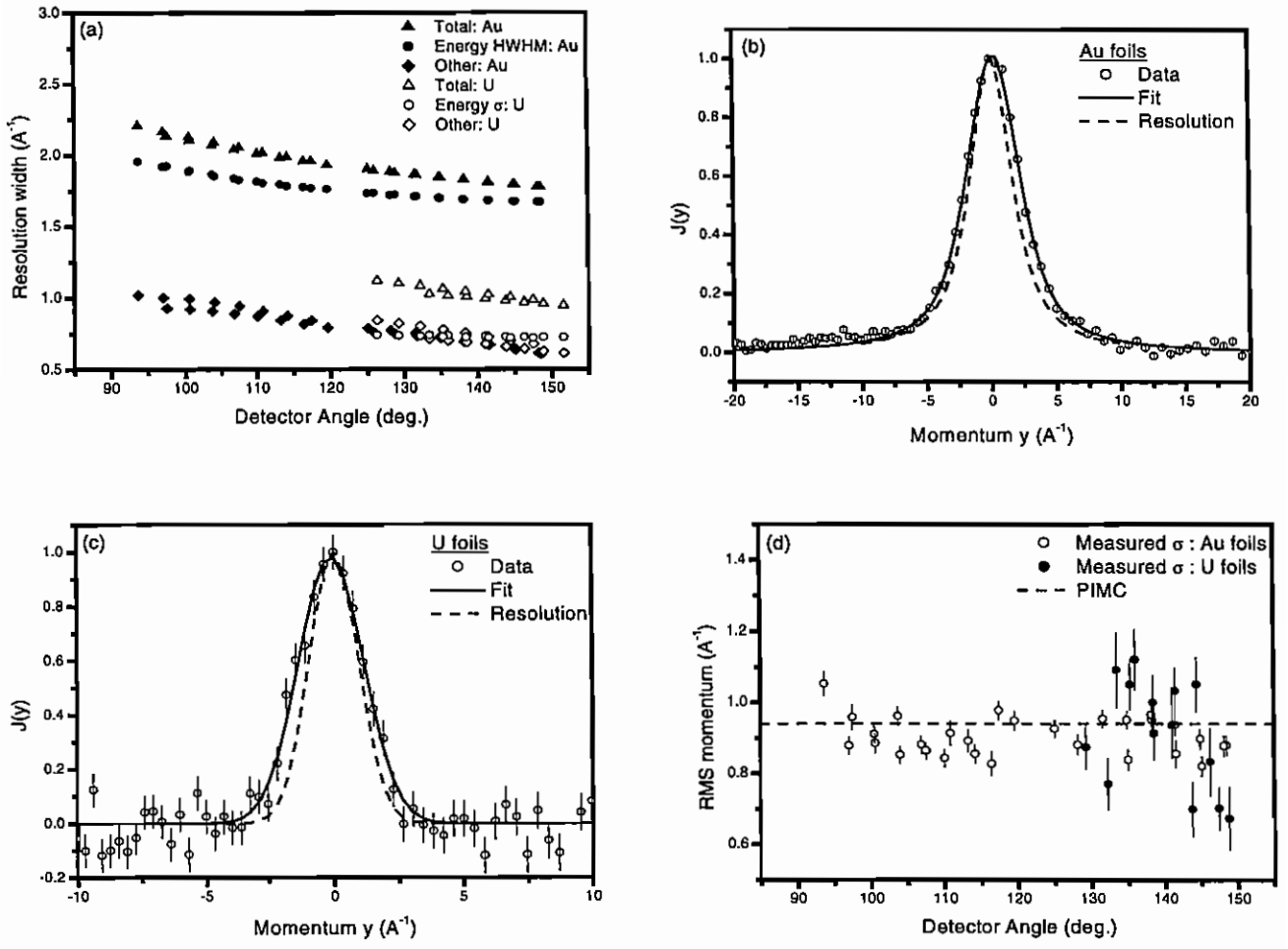

Figure 15 *(a) Resolution widths in momentum space for measurements made on ^{4}He at 2.5 K and SVP plotted as a function of scattering angle. The solid points represent measurements made using Au analyser foils and the hollow points represent measurements made using U analyser foils. (b) J(y) measured using Au analyser foils at a scattering angle of 145^o. The dashed line represents the resolution function in momentum space and the solid line represents the fit to the data. (c) J(y) measured using U analyser foils at a scattering angle of 147 ^{o}. The dashed line represents the resolution function in momentum space and the solid line represents the fit to the data. (d) The fit derived second moments of the neutron Compton profiles, J(y), plotted as a function of detector angle for both the data measured using Au and U analyser foils. The dashed line represents the value calculated using PIMC techniques.*

with the y-space resolution R(y) with the amplitude, peak position and standard deviation, σ, as free fit parameters. The fitted σ values are plotted as a function of scattering angle in figure 14(d) and the mean values for each bank of detectors listed in table 5. Good agreement is found between the values measured using Au and U foils and also with the value of 4.1 $Å^{-1}$ calculated in the harmonic model using the measured density of states [10]. The error bars in figure 14(d) are purely statistical errors that are derived from the standard fitting procedure and do not take account of any possible systematic errors. This could explain the scatter of the data points being more significant than the error bars.

5.2 Helium

Liquid helium-4 remains the most accessible pure Bose liquid in nature and a key model system. This is largely due to the transition it undergoes below a temperature of 2.17 K when the helium atoms condense into a state characterised by the macroscopic occupation of one single-particle quantum state. London [19] proposed that this Bose-Einstein condensate is the origin of superfluidity. The momentum distribution of liquid helium-4 was one of the first systems to be studied using the technique of neutron Compton scattering, the goal being to measure a change in the lineshape of the momentum distribution due to the condensate. The intrinsic width of the momentum distribution of ^{4}He is very narrow therefore extremely good resolution is required if accurate values for the single particle kinetic energies are to be measured. This makes normal phase ^{4}He a good system to validate the calibration procedures. We present here two sets of data that were measured using the eVS on liquid ^{4}He at saturated vapour pressure and a temperature of 2.5 K. One set of measurements was made using Au analyser foils, the other using U analyser foils. The two sets of measurements were made independently of one another and the calibration procedures described in this paper were used for both. Figure 15(a) shows the calibrated resolution widths as a function of scattering angle for both the U foil and Au foil measurements. The Compton profiles, J(y) measured at the highest scattering angle for the Au and U foils are plotted in figure 15 (b) and (c) respectively. Also plotted are the resolution functions R(y) and the fitted Gaussian J(y) convoluted with the resolution, R(y). The fitted second moment, σ, of the Compton profiles are plotted

(a)

Detectors	Scattering Angle	Mean σ (Å^{-1})
1 - 8	117 – 93 °	0.89 (0.02)
9 - 16	119 – 97 °	0.89 (0.02)
17 - 24	124 – 148 °	0.94 (0.01)
25 - 32	148 – 125 °	0.88 (0.02)
1 – 32	93 – 148 °	0.90 (0.01)

(b)

Detectors	Scattering Angle	Mean σ (Å^{-1})
17 – 2 4	133 – 151 °	0.85 (0.07)
25 - 32	147 – 126 °	0.89 (0.06)
17 - 32	126 – 147 °	0.87 (0.04)

Table 6 *The mean second moments of the measured Compton profiles of ^{4}He for each bank of detectors using (a) Au analyser foils and (b) U analyser foils.*

as a function of the scattering angle in figure 15(d) for both the Au and U foil measurements. Plotted as a straight dashed line is the value of 0.94 Å^{-1} that was calculated using Path Integeral Monte-Carlo (PIMC) methods [20]. The mean values for each detector bank are listed in table 6 where excellent agreement is seen between the two independent measurements using different analyser foils. These values are also in agreement with previous measurements made using chopper spectrometers [21] as well as the PIMC calculations.

5.3 Tin

Measurements were made on a 1 mm thick sample of tin using uranium analyser foils. The measurements were made as part of a series of measurements to investigate multiple scattering in eVS measurements. However, the dataset provides a good example of an eVS measurement that is resolution limited. The reason for this is that

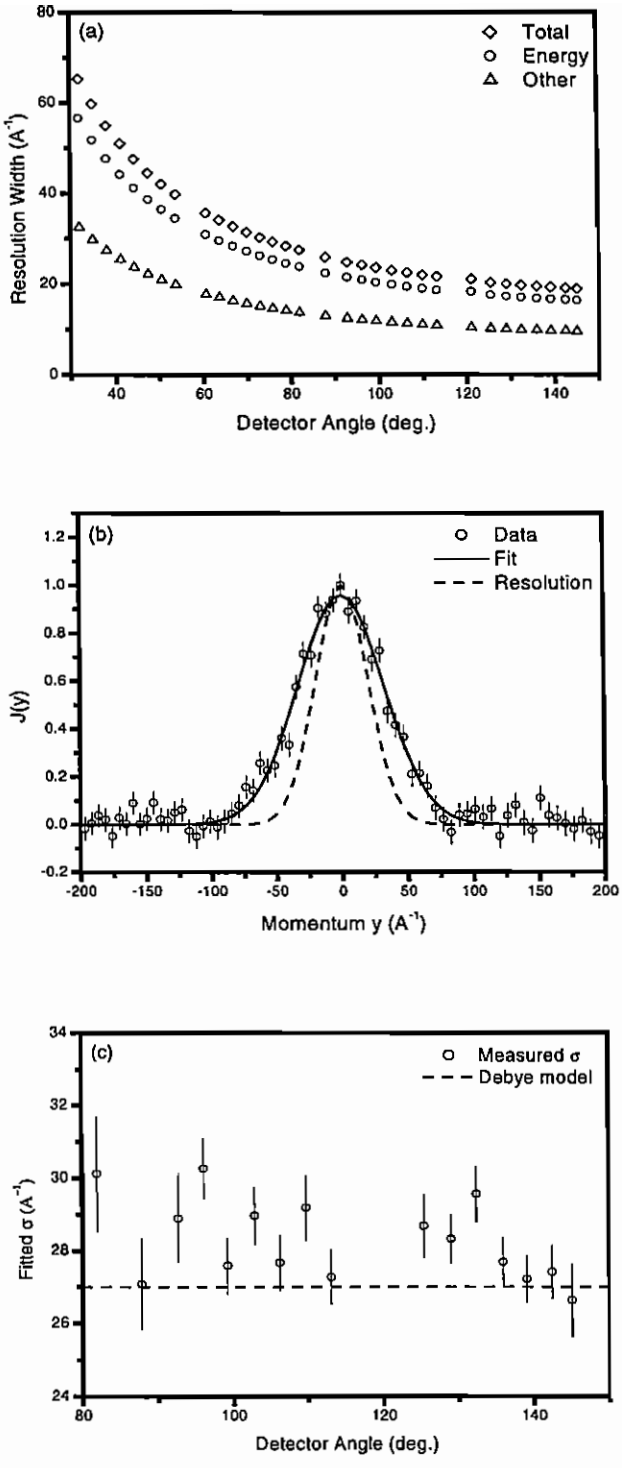

Figure 16 *(a) Resolution widths in momentum space for measurements made on a 1 mm thick sample of tin at room temperature plotted as a function of scattering angle. U analyser foils were used. (b) J(y) measured at a scattering angle of 145 °. The dashed line represents the Gaussian resolution function and the solid line represents the fit to the data. (c) The fit derived second moments of the measured neutron Compton profiles plotted as a function of detector angle. The dashed line represents the value calculated using the Debye model.*

Detectors	Scattering Angle	Mean σ ($Å^{-1}$)
17 – 24	121 – 145 °	27.68 (0.35)
25 - 32	87 – 113 °	27.91 (0.38)
17 - 32	87 - 145	27.81 (0.25)

Table 7 *The mean second moments of the measured Compton profiles of Sn for each of the two high angle detector banks.*

the eVS resolution gets progressively worse as the atomic mass increases. Measurements on the heavy Sn atoms therefore are on the limits of instrument resolution and provide a good test of the calibration procedures. The widths of the resolution function in momentum space are plotted in figure 16(a), only data measured at scattering angles above 80° are reliable as below this the resolution deteriorates rapidly. The data were analysed using standard eVS analysis routines that fit a Gaussian J(y) convoluted with the resolution R(y). Figure 16(b) plots a Compton profile measured at the highest scattering angle (θ = 145°), also plotted are the Gaussian resolution function and the fit to the data. The fitted second moments of the Compton profiles are plotted in figure 16(c) as a function of scattering angle and listed in table 7, the dashed line is the RMS momentum calculated using the Debye model.

6. **Discussion & Conclusions**

The aim of this paper has been to describe the procedures that are used to calibrate the electron Volt spectrometer at the ISIS neutron spallation source. The spectrometer currently has four modules of detectors that can be moved to cover scattering angles ranging from 30° up to 145° depending on the requirements of a particular experiment. There is also the option to use gold or uranium analyser foils. The instrument must therefore be re-calibrated each time the detectors are moved or the analyser foils changed. The procedures in this paper show how this can be done accurately and simply, in a few hours if necessary, by making just two calibration measurements on a Pb sample. The methods used to define the contributions to the

instrument resolution function have also been shown using a combination of the Pb calibration measurements and Monte-Carlo calculations. Examples of neutron Compton scattering measurements on 3 different systems, hydrogen, helium and tin have illustrated that the procedures work well and that accurate and consistent values for the atomic kinetic energies can be derived.

---

[1] M. Celli, M. Zoppi and J. Mayers Phys. Rev. B **58** 242 (1998)

[2] J. Mayers, C. Andreani and D. Colgonesi J. Phys.: Condens. Matter **9** 10639 (1997)

[3] D.N. Timms, A.C. Evans, M. Boninsegni, D.M. Ceperley, J. Mayers and R.O. Simmons J. Phys. Condens. Matter **8** 6665 (1996)

[4] P. Postorino, F. Fillaux, J. Mayers, J. Tomkinson and R.S. Holt J. Chem. Phys. **94** 4411 (1991)

[5] S. Fulton, R.A. Cowley and A.C. Evans J. Phys.: Condens. Matter **6** 2977 (1994); A.C. Evans, J. Mayers and D.N. Timms J. Phys.: Condens. Matter **6** 4197 (1994)

[6] J. Mayers Phys. Rev. Lett. **71** 1553 (1993); U. Bafile, M. Celli, M. Zoppi and J. Mayers Phys. Rev. B **58** 791 (1998); C. Andreani, D. Colgnesi , A. Filabozzi, E. Pace and M. Zoppi J. Phys. Condens. Matter **10** 7091 (1998)

[7] F.J. Bermejo, F.J. Mompean, A.Srinivasan, J. Mayers and A.C. Evans Phys. Lett. **189A** 333 (1994)

[8] A.L. Fielding, D.N. Timms, J. Mayers Europhysics Letters **44** 255 (1998)

[9] S.X. Zeng, R.O. Simmons, D.N. Timms and A.C. Evans J. Chem. Phys. **110** 1650 (1999)

[10] A.C. Evans, D.N. Timms, J. Mayers and S.M. Bennington Phys. Rev. B **53** 3023 (1996); A.L. Fielding, D.N. Timms, A.C. Evans and J. Mayers J. Phys.: Condens. Matter **8** 7205 (1996); E.M.A Gray, M. Kemali, J. Mayers and J. Noreland Journal of Alloys and Compounds **253-254** 291 (1997)

[11] P.C. Hohenberg and P.M. Platzmann Phys. Rev. **152** 198 (1966)

[12] G.B. West Phys. Rep. **18C** 263 (1975)

[13] C.G. Windsor *Pulsed Neutron Scattering* 1981 (London: Taylor and Francis)

[14] G.L. Squires *Introduction to the theory of thermal neutron scattering* 1996 (Dover)

[15] S.H. Mughabghab and D.I. Garber. Neutron Cross-sections vol. 1.

[16] C. Andreani, G. Baciocco, R.S. Holt and J. Mayers Nucl. Instr. Meth. Phys. Res. **A276** 297 (1989)

[17] P.A. Seeger, A.D. Taylor and R.M. Brugger Nucl. Instr. Meth. Phys. Res. **A240** 98 (1985)

[18] J. Mayers, T.M. Burke and R.J. Newport J. Phys.: Condens. Matter **6** 641 (1994)

[19] F. London, Nature **141** 643 (1938); Phys. Rev. **54** 947 (1938)

[20] D.M. Ceperley and E.L. Pollock Can. J. Phys. **65** 1419 (1987)

[21] T.R. Sosnick, W.M. Snow, P.E. Sokol and R.N. Silver Phys. Rev. B **41** 11185 (1990)